

LOCATING LOSSES DUE TO CONTACT RESISTANCE, SHUNTS AND RECOMBINATION BY POTENTIAL MAPPING WITH THE CORESCAN

A.S.H. van der Heide

J.H. Bultman

J. Hoornstra

A. Schönecker

G.P. Wyers

W.C. Sinke

This paper has been presented at the 12th NREL Workshop on crystalline silicon solar cells,
materials and processes, Breckenridge (CO), USA, 11-14 August 2002

Locating losses due to contact resistance, shunts and recombination by potential mapping with the Corescan

A.S.H. van der Heide, J.H. Bultman, J. Hoornstra, A. Schönecker, G.P. Wyers, W.C. Sinke
ECN Solar Energy
P.O. Box 1, 1755 ZG, Petten, The Netherlands
Phone: +31 224 564723; Fax: +31 224 568214
E-mail: vanderheide@ecn.nl

Abstract

A visualization tool to locate losses in a solar cell can be very helpful in troubleshooting a non-optimal production line. Therefore, the Corescan has been developed, in which three different locating methods are incorporated, the Corescan, Shuntscan and the new V_{oc} scan. In this paper it is explained how the scan results have to be interpreted and it is shown that the sensitivity of the methods is more than sufficient. The unique V_{oc} scan method is introduced for the first time; this technique can locate recombination losses on cells that are almost complete (only the front contact has to be omitted). Several examples of how the Corescan instrument can be used for troubleshooting and process optimization are presented in this paper. These examples will help users of the instrument to relate measured scans with reasons for non-optimal processing.

Introduction

Normally, standard $J-V$ measurements are used to determine whether a production line is running properly. The process engineer must react when the $J-V$ fit results get below or above a certain threshold. The $J-V$ fit parameters themselves do not always reveal the real loss mechanism responsible for off-spec functioning of the process line, apart from loss due to shunts. It is difficult to determine whether a drop in fill factor is due to series resistance or recombination loss (see the Appendix and [1]). To distinguish between series resistance and recombination, an additional open circuit voltage measurement as a function of light intensity [2] is necessary. This separation of different loss sources is important, but not enough in itself to determine the real cause(s) for a lowered fill factor. This is much easier to do when also the loss locations on the cell can be determined for the different loss mechanisms.

A new way to find the loss locations has been presented recently [1,3]. The basic principle is to map the potential distribution on the front side of a solar cell, while operating the cell at conditions that enable separation of a specific loss type from the others. Using different conditions, it is possible to locate either losses due to series resistance (most importantly contact resistance), to shunts or to high recombination. These methods were patented [3] and incorporated in the Corescan, developed for industrial use and commercially available. The instrument is shown in Fig. 1. More details and on-line versions of Corescan publications are available at [4]. Corescan is derived from COnTact REsistance scan, since

this is the most important scan mode. The three different scan modes of the Corescan are called Corescan, Shuntscan and V_{oc} scan.

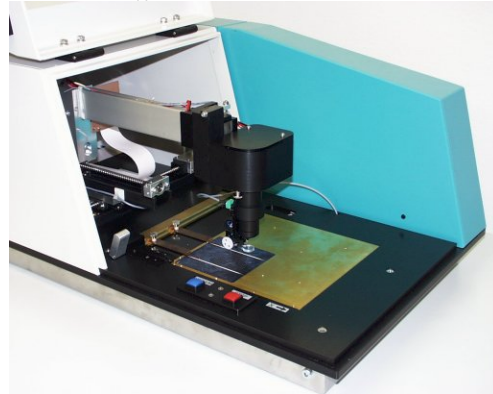


Figure 1: Corescan instrument

The Corescan method is the only method that is able to determine the contact resistance over the entire cell surface. It has shown to be a very important and helpful tool, which makes reduction of the front side contact resistance easy. In case of contact problems it was found that the contact resistance is mostly very non-uniform. The distribution by itself can often be used to deduce the reason for poor contact.

The Shuntscan method is one of the few that is sensitive enough to enable shunt locating at the right (=forward) bias polarity. The main advantages compared to other forward bias methods, contact thermography [5], lock-in IR thermography [6] and CASQ [7], are the relative simplicity and lower costs of the Shuntscan.

The V_{oc} scan method will be presented here for the first time. It gives important information about differences in local diode behaviour over the cell. This method only works optimally when the front side metallization is omitted.

This paper discusses these three different potential mapping methods of the Corescan as well as their use in troubleshooting process optimization.

Corescan method

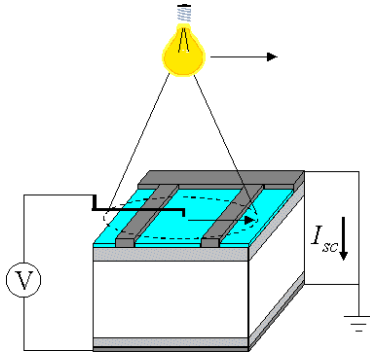


Figure 2: Schematical drawing Corescan method

The Corescan method (see Fig. 2), uses the fact that series resistance sources can be detected by potential differences that occur over these resistances while current is flowing in the device. In the Corescan, the current is generated by application of illumination while the cell is short-circuited externally. The potential at the front side is measured with a metal probe in direct contact with the surface, that is scanned across the cell. The size of the illuminated spot around the potential probe is not critical, as long as it is not smaller than a few finger separations. The contact resistance of a finger is proportional to the potential jump V_{ce} across the contact interface at the edge of the finger. This jump is the difference between the potential at the metal finger and the first point on the silicon adjacent to it (see Fig. 3). The proportionality factor is $1/i_c$, where i_c is the current flowing through the contact interface per unit length of finger. In formula form:

$$R_{cl} \equiv \frac{V_{ce}}{i_c} = \frac{V_{ce}}{dJ_{sc}},$$

where R_{cl} is the line contact resistance, J_{sc} is the short circuit current density within the beam and d is the distance between two fingers.

This line contact resistance is used instead of the more usual specific contact resistance ρ_c , because ρ_c is not so appropriate for screen printed contacts. This is because calculating ρ_c correctly involves the emitter sheet resistance below the finger and the assumption of a constant ρ_c across the finger width. However, the emitter sheet resistance below screen printed fingers increases to an unknown value during sintering due to dissolving of silicon, and the contact interface is very non-uniform. Instead of trying to separate the influence of ρ_c and emitter sheet resistance, the definition of R_{cl} includes both parameters in a single value. In fact, this is the only value of importance for the current output of the cell region between the fingers.

In the Corescan instrument, for practical reasons local illumination is used, the diameter of the beam is 9 mm. The probe is scanned perpendicular to the fingers with a resolution of 0.1 mm so that no finger is missed. To scratch through the isolating anti-reflection coating that is usually present on the front surface, the probe is continuously in contact with the surface during the scan and is made of a hard material (tungsten). By performing scan lines with a separation of 2 mm, it is possible to

obtain a potential map of the entire cell, which takes about 6 min for a 10 x 10 cm cell. An example of a scan line part is shown in Fig. 3.

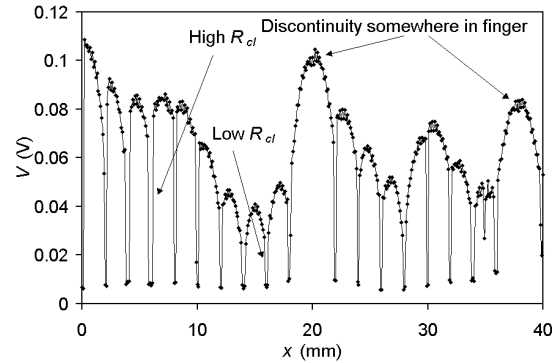


Figure 3: Part of one Corescan scan line

The potential jumps at the fingers due to contact resistance are clearly visible; the large spread in R_{cl} that is found on this cell is typical for cells that have a contact problem. The influence of other series resistance sources is also visible: the emitter sheet resistance causes a parabolic potential behaviour between the fingers and a finger discontinuity causes an effectively doubled finger spacing. The large non-uniformity of R_{cl} that is often found on solar cells causes high diode factors or second diode currents when fitting the J - V curves, as is explained in the Appendix.

The minimum contact resistance that can be measured with the Corescan instrument can be calculated from the minimum measurable V_{ce} and maximum J_{sc} for the instrument. These values are 2 mV and 60 mA/cm², so for a typical finger spacing of 2 mm, the minimum R_{cl} is $\sim 0.2 \Omega\text{cm}$. For reference: this would correspond to $\rho_c \sim 2 \text{ m}\Omega\text{cm}^2$, assuming a constant ρ_c across the finger width and assuming a sheet resistance below the finger of 100 Ω . This accuracy of the Corescan is more than sufficient, since the influence of such a low contact resistance is negligible for illuminations up to 1 sun.

Before the Corescan method was developed, contact resistances could only be determined with the Transmission Line Model (TLM) method [8]. The TLM method is schematically shown in Fig. 4. The resistance is measured between one finger and other adjacent fingers. From the graph of resistance against distance, the emitter sheet resistance and contact resistance can be determined.

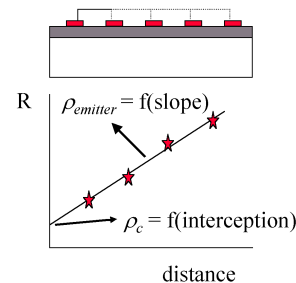


Figure 4: Principle TLM method

When the sheet resistance and contact resistance are assumed to be constant (which is often not the case), the points will be located on a straight line with a slope proportional to the sheet resistance and an intersection with the resistance axis proportional to the contact

resistance. The fingers have to be disconnected from the busbar to prevent parallel conduction. In practice this is usually done by laser cutting.

The advantages of the Corescan compared to TLM are that it is not necessary to assume the contact resistance to be the same for all fingers, it is not necessary to cut the cell, and the entire surface can be quickly measured.

Corescan application

In this section, Corescans will be shown for different causes of high (and non-uniform) contact resistance.

In the first example, 10 x 10 cm multi-crystalline silicon solar cells with silicon nitride were fired at different temperatures around an optimum value T . Contacts were applied by screen printing and co-firing of aluminum paste on the back side and silver paste on the front side. The cells are positioned on the belt with the busbars perpendicular to the belt direction.

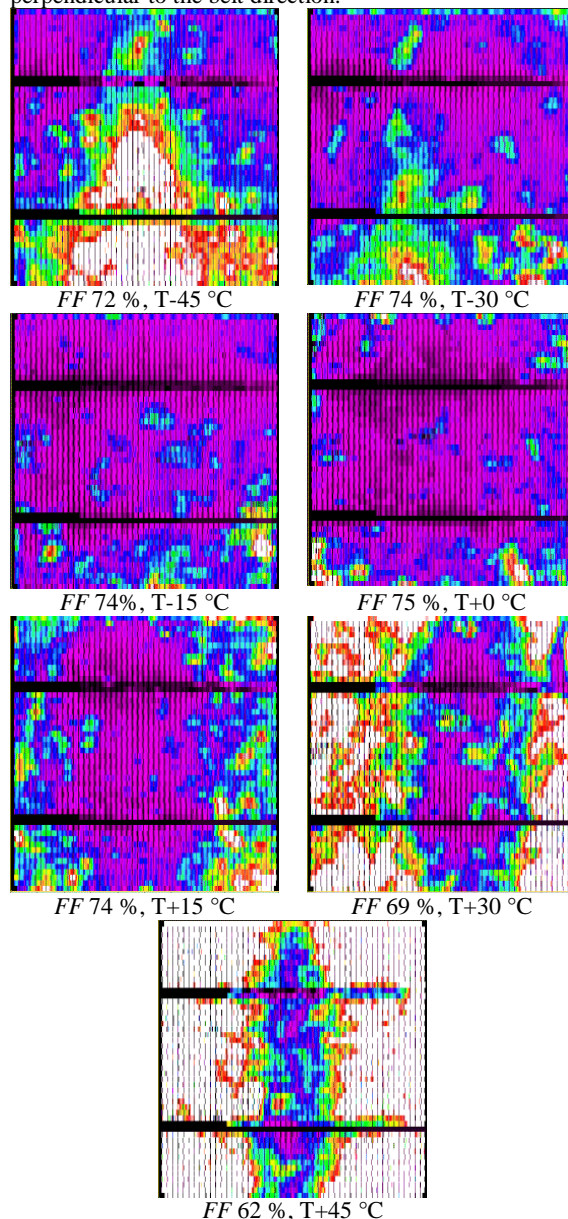


Figure 5: Corescans on cells fired at different set temperatures. Lighter areas have higher potential and thus higher contact resistance.

These scans show a large non-uniformity in R_{cl} which is due to cross-belt temperature differences. The middle region is the coolest: in this region it is too cold for good contact formation at low firing temperature, while it is the only region that has still good contact at high firing temperatures. This was enough reason to study the design of the furnace.

In IR firing furnaces, the belt is supported by fused quartz rods oriented in parallel with the belt direction. The IR lamps used for heating the cells are situated both above and below the belt. When the lamps below the belt are used, IR radiation will be blocked to some degree by the support rods, which could explain the observed temperature non-uniformity. By changing the position of cells during firing with respect to the support rod the high contact resistance region shifted over the cell. Therefore the conclusion was drawn that the center rod blocked too much IR radiation from the lamps below the belt.

Another example of temperature differences leading to R_{cl} uniformity is shown in Fig. 6. A Corescan is shown for a cell fired in a furnace with a belt with small quartz product supports. These support the products on the belt to prevent direct belt contact, and were suspected to cause contact resistance non-uniformity.

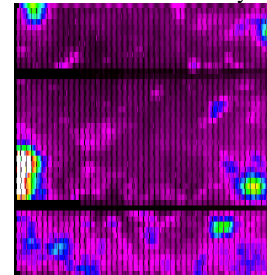


Figure 6: Corescan of a cell fired in a belt furnace, on a belt having quartz product supports. The positions exactly coincide with the supports.

It is clear from the Corescan that the temperature was too low indeed for good contact formation at the locations of the quartz product supports.

An emitter related contact problem is shown in Fig. 7, where a circle of increased contact resistance is visible.

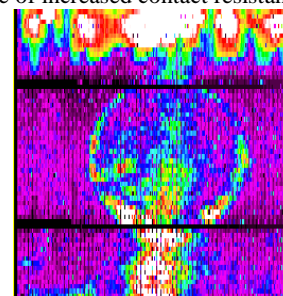


Figure 7: Circle of increased contact resistance due to locally less doped emitter

This circle is caused by application of dopant on the cell by spinning of a phosphorus containing fluid on both sides (the back side is overcompensated with aluminum later on). On the surface that was spun first, some fluid has been removed at the circle when dopant was applied to the second surface. Due to less dopant fluid the emitter resistance is increased, apparently to a value too high for good contact formation. Although this particular example may not be a very usual one, it is a good illustration of the effect of emitter non-uniformity, that can also be caused otherwise. These lateral doping variations become

especially important when lighter doped emitters are used in order to reduce recombination losses in the emitter. The next example is a contact problem caused by plasma etching of the solar cell edges for isolation (see Fig. 8).

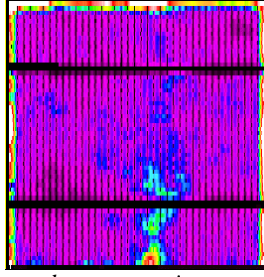


Figure 8: Increased contact resistance at the edges due to some emitter removal during plasma etching for edge isolation

The figure shows that the contact resistance is clearly increased near the edges of the front surface. Apparently some of the emitter on the front surface has been removed during the plasma etching, which was done immediately after emitter diffusion.

Some other causes for R_{cl} non-uniformity that have been identified so far are incomplete phosphorus glass removal, the presence of contamination on the silicon before contact firing, non-uniform TiO_x coating [1] and too low and non-uniform screen print pressure due to a wear dip on the screen printer vacuum chuck [9].

Shuntscan method

For the Shuntscan, the current necessary to detect shunts is generated by applying a bias across the cell with a power supply (see Fig. 9).

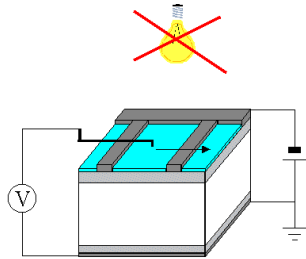


Figure 9: Drawing of the Shuntscan method

In order to study only shunt current flow, current generation by light is avoided by measuring in the dark. The current flowing through a shunt is supplied by the surrounding emitter area, and because the sheet resistance of the emitter is considerable, a potential decrease in the direction of the shunt will exist. In a Shuntscan this local potential decrease is detected; the magnitude of the shunt can be calculated from the potential gradients around it and the emitter sheet resistance.

To find the shunts that are important for the cell at normal operation, it is necessary to apply a forward bias to the cell. The reason is that not all shunts in solar cells are ohmic [10], so that shunts detected in reverse bias may not be shunts in forward bias. It is important to note that the Shuntscan is sensitive enough to detect shunts at forward bias. Except for lock-in techniques, the other methods that use heat detection to locate shunts have to use reverse bias to induce sufficiently high shunt

currents. This is used for example in case of detection with liquid crystals. The magnitude of the forward bias applied during the Shuntscan is adjustable; ideally it should be around the maximum power point (~0.5 V), but since the scratching of the probe itself induces some extra diode current due to surface damage it is better to use ~0.3 V. At that potential the diode is not conducting (even when scratched) and all currents are caused by shunts.

To calculate the current detection limit for the Shuntscan, the potential distribution $V(r)$ around a shunt must be calculated. To simplify the calculation, it is assumed that there are no fingers and that the cell is infinitely large. After the calculation for this simplified case, the influence of deviations of this model in case of real cells will be discussed.

The current flow to the shunt will be circle symmetric; the horizontal current i flowing in the emitter through a unit width is related to the shunt current I_{sh} and the distance r from the shunt (located at $r = 0$) by

$$i = \frac{I_{sh}}{2\pi r},$$

since the total current crossing the edge of any circle centered around the shunt is always I_{sh} (no current is lost).

The magnitude of i is Jt , where J is the current density of the horizontal current flow in the emitter with thickness t . At the current densities occurring in a solar cell, J is proportional to the electric field $E (= dV/dr)$ and the conductivity $\sigma (= 1/\rho)$, where ρ is the resistivity):

$$J = \sigma E = \frac{1}{\rho} \frac{dV}{dr}$$

So i can be expressed in terms of dV/dr as follows:

$$i = tJ = \frac{t}{\rho} \frac{dV}{dr} = \frac{1}{\rho_s} \frac{dV}{dr},$$

where ρ/t has been substituted by the emitter sheet resistance ρ_s .

Combining the expressions for i gives the following differential equation for $V(r)$:

$$\frac{dV}{dr} = \frac{\rho_s I_{sh}}{2\pi} \frac{1}{r},$$

which has the general solution

$$V(r) = \frac{\rho_s I_{sh}}{2\pi} \ln r + C.$$

As an example, $V(r)$ is drawn for two different I_{sh} values in Fig. 10.

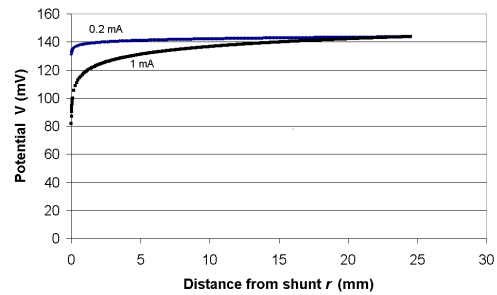


Figure 10: $V(r)$ for 2 different I_{sh} values; $\rho_s = 50 \Omega$

The shunt with the larger I_{sh} clearly has a much larger area with lower potential around it.

The current detection limit of the Shuntscan can now be estimated; the smallest shunt that can be detected is determined by the smallest potential difference that can be detected when moving from “the shunt” to $r = 1.0$ mm (to stay between the fingers on a real cell). “The shunt” means here the point as close as possible to it, since the potential probe itself has a finite diameter (in this case 0.2 mm). Taking r ‘at shunt’ = 0.1 mm, r ‘far away’ = 1.0 mm, $\rho_s = 50 \Omega$ and minimum $\Delta V = 5$ mV, the minimum detectable current for a single shunt turns out to be ~ 0.25 mA. Compared to a current at the maximum power point of a 10 x 10 cm cell of 3 A, this would mean 0.01 %, so that the sensitivity for a single shunts on an otherwise non-shunted surface is more than sufficient.

In practice, the ideal case of current flow only through one shunt and no current flow elsewhere does not exist. There will always be a small more or less homogeneous background, which cannot be detected by the Shuntscan. Therefore, the shunt resistance limit below which shunts will be found on a cell with the Shuntscan is lower than would be expected from this single shunt case. As a rule of thumb, cells with a shunt resistance below 1-2 $k\Omega cm^2$ are found to be interesting for Shuntscan investigation. This corresponds to the limit below which shunts have significant influence on the cell efficiency, so the Shuntscan sensitivity is also enough on real cells.

In the case of a shunt at the Shuntscan detection limit of only 0.25 mA, the radius of influence is very small. Therefore, the potential distribution will not be much disturbed by the fingers that are present on real cells. However, when a shunt is larger, the potential distribution will be disturbed by the fingers, the degree of disturbing mainly depends on the contact resistance of the fingers around the shunt. The reason is that fingers are much better conducting than the emitter, and when the fingers around the shunt can supply enough current for the shunt, there is no flow of current in the emitter outside these fingers. An example of this is shown in Fig. 11, where the potential dip of 80 mV would be large enough to have a considerable influence radius without fingers (compare with Fig. 10).

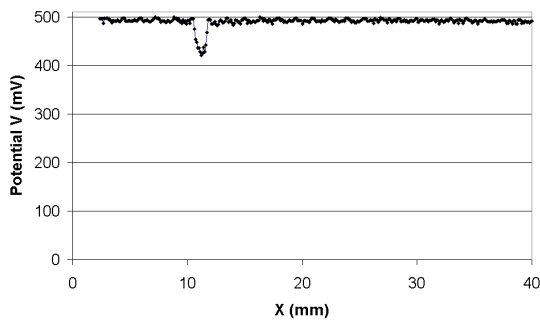


Figure 11: Confined influenced area by easy current supply by the fingers in case of low contact resistance.

However, when the fingers have a considerable contact resistance they cannot easily supply current for the shunt and the situation will be more like the one calculated without fingers. An example of this case is shown in Figure 12.

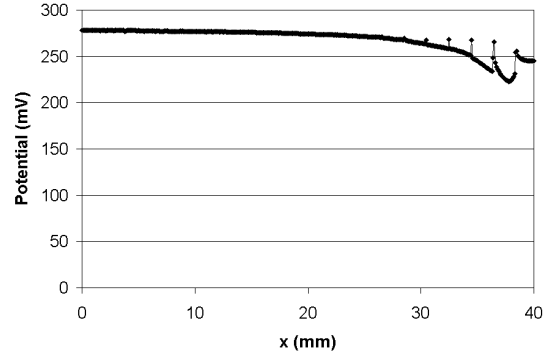


Figure 12: Potential distribution around shunt for large contact resistance, in this case the potential is more like the one without fingers.

In fact, a shunt is somewhat shielded if the fingers around it have a large contact resistance, reducing to some extent the current loss due to the shunt. This is comparable to the shielding of a shunt by emitter sheet resistance which was discussed recently in [11]. In that paper the influence of contact resistance was not taken into account.

Comparing Figs. 11 and 12, it is clear that the area with lowered potential around a shunt is not a good measure for the shunt magnitude on real cells. Another point to note is that the potential dip is not very sharp in Fig.12. This is probably due to the fact that the probe was not scanned exactly across the shunt; the probe diameter of 0.2 mm also prevents the measurement of a very sharp peak.

Although actual potential distributions will always differ depending on the exact shunt location and metallization properties, it is in principle always possible to calculate the total current flowing through a shunt. The method is to perform a path integration of i along any closed path around the shunt that does not include a finger part:

$$I_{sh} = \oint \vec{i} \cdot \hat{n} ds = \frac{1}{\rho_s} \oint \nabla V \cdot \hat{n} ds .$$

i is written here in vector form and its inproduct with the inward normal to the integral path is taken, to account for the fact that i will generally not be perpendicular to the integral path (in the circle symmetric case, vector magnitudes were sufficient since i was perpendicular to the circle everywhere).

In practice, it is difficult to calculate the integral accurately since a very high lateral resolution is needed for the measurement of V in both x and y direction. However, a rough estimate which is sufficient for most purposes can be made with it.

In the near future, some detailed measurements will be made in an experiment to compare the absolute shunt current found with lock-in IR thermography with the value found with the Shuntscan.

To summarize, the Shuntscan can detect shunts at forward bias with sufficient degree of accuracy. It has been shown that the area with lowered potential around a shunt is not a good measure of its magnitude on a real cell, because the contact resistance of surrounding fingers is of influence as well. It is explained that the Shuntscan potential data can be used for quantitative analysis of shunts. In practice, the Shuntscan is mostly used in a qualitative way, some examples will be given in the next section.

Shuntscan application

Using the Shuntscan, several types of defects have been identified so far. In Fig. 13, a Shuntscan made on a 10 x 10 cm cell having a shunt resistance of $500 \Omega\text{cm}^2$ is shown.

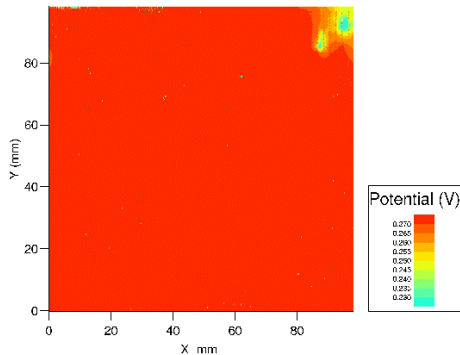


Figure 13 : Shuntscan on a multicrystalline silicon cell with shunts in the upper right corner.

It is clear that there are several shunts between the fingers in the upper right corner of the cell. After this corner was removed, the resistance increased to $3000 \Omega\text{cm}^2$, which is an acceptable value. In this case, the problem was probably base material related, e.g. SiC precipitates could be the reason.

In another experiment, both a Shuntscan and lock-in IR thermography picture were made for the same cell (see Fig. 14).

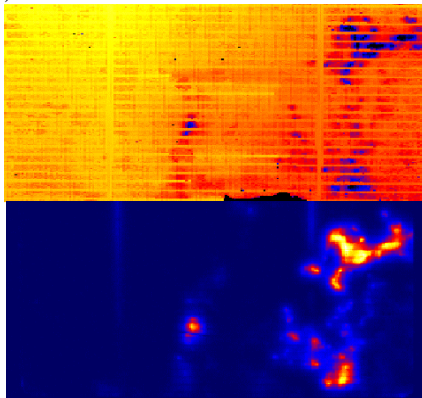


Figure 14: Comparison Shuntscan (upper picture) and lock-in IR thermography. The colors are inverted because a decrease in potential in the Shuntscan corresponds with an increase of the temperature measured by lock-in IR thermography.

It is clear that the methods agree about the shunt locations. The only difference is that shunts below metallization cannot be detected by the Shuntscan because the resistance of the metal is too low, while the heat produced by a shunt can be detected by lock-in IR thermography also below metal. An example of this is visible in Fig. 14 at the right busbar. For the cell in Fig. 14, the shunts were found to be due to material problems in the silicon base material, since scans on neighbouring wafers have shunts on the same locations.

Typical process related problems that were found on other cells are poor edge isolation, metal contamination on the front side of the cell and cracks.

V_{oc} scan method

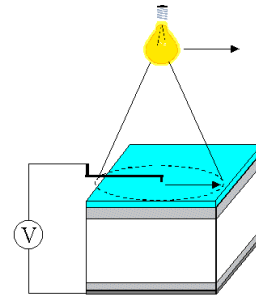


Figure 15: Drawing of the V_{oc} scan method

The V_{oc} scan principle (see Fig. 15) is simple and straightforward. A potential probe centered in a light beam is scanned over the front surface of a cell without front side metallisation, while the cell is in open circuit condition. The metallization has to be omitted to avoid smearing out of the potential. Although the scratching of the cell has been found to cause some V_{oc} loss by scanning a second time, the same distribution pattern is found again, so in that sense the result is reproducible.

With the V_{oc} scan, a kind of local V_{oc} is measured, although the values measured can be considerably lower than for uniform illumination. The reason is that the light current generated in the beam can leak to the dark area around it. This effect is not present in case of uniform illumination, because the diode current at each location is compensated by the light current generated at the location itself. Lateral currents are therefore avoided and the local potentials reach higher values.

The result is that potential differences measured with the V_{oc} scan are exaggerated compared to the case of uniform illumination. The advantage is that differences are clearly visible; on the other hand, the current leakage makes the analysis of the scan method in a quantitative way difficult. Up till now, the V_{oc} scan has only been used as a qualitative tool.

V_{oc} scan application

In Fig. 16, the influence of the local absence of a back surface field (BSF) as measured by a V_{oc} scan is shown. The cell without front contact was fabricated with an aluminum back side, except for the regions at the back below the busbars, where silver was printed for soldering.

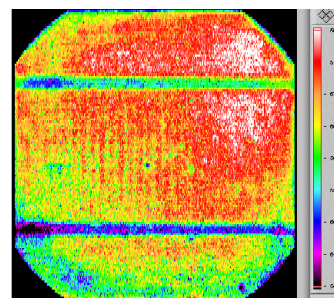


Figure 16: V_{oc} scan for a mono-crystalline cell. The potentials on the cell cover the entire color scale on the right, ranging from 540 to 580 mV.

V_{oc} is lower at the 'back side busbars' where no aluminum is present, due to less gettering and/or an

absence of BSF at these regions. In addition, V_{oc} on this cell turns out to be slowly increasing to the upper right, caused by emitter or BSF non-uniformity.

In another experiment, acid etched multi-crystalline cells were fabricated, among them some without front contact. The neighbouring complete cells had high J_{sc} values, but a low FF . A V_{oc} scan on one of the cells without front contact and a picture of the cell are shown in Fig. 17.

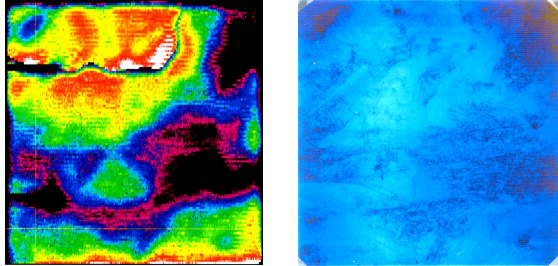


Figure 17: V_{oc} scan and picture for an acid etched cell. The coincidence between low V_{oc} (black regions) and etched defects is clear.

The scan demonstrates that areas where defects have caused extra etching are mainly responsible for the FF loss, since the measured V_{oc} is lower in these areas. A dark crack is also visible in the upper part of the scan, while it was not visible on the cell.

As the V_{oc} scan method is presented here for the first time, not many cells have been studied yet. However, these first results show that also the V_{oc} scan is a promising method for process optimization.

Conclusions

The different techniques based on potential mapping used by the Corescan are able to locate losses due to contact resistance, shunts and recombination in solar cells. The sensitivities of the methods are sufficient to find all significant locations.

An important fact found with the Corescan is that the cross-belt temperatures differences in a belt furnace can be significant, resulting in non-uniform contact resistance.

With the Shuntscan, shunts were detected related to base material problems, metal contamination and edge isolation problems. The influence of fingers on the measured potential distribution around a shunt was discussed, as well as the quantification of shunt current from measured potentials around a shunt.

The principle of the newly developed V_{oc} scan was explained, as well as its interpretation. With this V_{oc} scan, the influence of the local absence of a BSF on the back side was demonstrated. Acid texturization was found to be responsible for local fill factor loss of the silicon diode itself at defect locations visible by eye.

Summarizing, the Corescan instrument, equipped with the Corescan, Shuntscan and V_{oc} scan, has proven to be a valuable tool for troubleshooting and process optimization in industrial solar cell processing.

References

- [1] A.S.H. van der Heide, A. Schönecker, G.P. Wyers, W.C. Sinke, 16th *European Photovoltaic Solar Energy Conference*, Glasgow (United Kingdom), 1438 (2000)
- [2] R.A. Sinton, 9th NREL workshop on crystalline silicon solar cell materials and processes, Breckenridge (Colorado, USA), 67 (1999)
- [3] A.S.H. van der Heide, Dutch patent 1013204, priority date 4 October 1999, patent granted 5 April 2001, worldwide patent pending
- [4] <http://www.sunlab.nl>
- [5] O. Breitenstein, W. Eberhardt, K. Iwig, 1st *World Conference on Photovoltaic Energy Conversion*, Hawaii (USA) 1633 (1994)
- [6] M. Langenkamp and O. Breitenstein, 9th NREL workshop on crystalline silicon solar cell materials and processes, Breckenridge (Colorado, USA), 198 (1999)
- [7] J. Kabs and H.J. Möller, *Proceedings 14th European Photovoltaic Solar Energy Conference*, Barcelona (Spain) 2381 (1997)
- [8] G.K. Reeves, H.B. Harrison, *IEEE Electron Device Letters*, 3, 111 (1982)
- [9] A.S.H. van der Heide, J.H. Bultman, J. Hoornstra and A. Schönecker, 12th *Photovoltaic Science and Engineering Conference*, Jeju (Korea), 591 (2001)
- [10] A. Kaminski, M. Langenkamp, O. Breitenstein, 14th *European Photovoltaic Solar Energy Conference*, Barcelona (Spain), 830 (1997)
- [11] J. Dicker, J. Isenberg and W. Warta, 17th *European Photovoltaic Solar Energy Conference*, Munich (Germany), 1567 (2001)
- [12] S. Bowden and A. Rohatgi, 17th *European Photovoltaic Solar Energy Conference*, Munich (Germany), 1802 (2001)

Appendix

An important consequence of the fact that R_{cl} is often found to be quite non-uniform is that the standard models to fit J - V curves of solar cells are not capable to include recombination and series resistance in the right fit parameters. A clear demonstration of this effect is shown in Figure A.1, where the J - V curve is calculated for a hypothetical cell having a region with good contact and an equally large region with bad contact. The applied method is to calculate J - V curves for the area between two fingers for both a low R_{cl} and a high R_{cl} and averaging these J - V curves. Averaging is done by taking $(J_{low R_{cl}} + J_{high R_{cl}})/2$ at each potential. The two curves are calculated assuming that the region between the fingers can be described by the following position-independent parameters: diode factor $m = 1.3$, $V_{oc} = 590$ mV, emitter sheet resistance = 50 Ω .

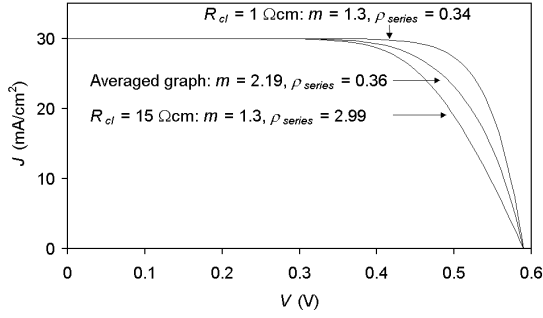


Figure A.1: Calculation of influence non-uniform R_{cl} on the J - V curve and fit parameters for a hypothetical cell having a region with good contact and a region with bad contact.

All curves were fitted and the parameters of the curves are indicated in the figure. It is found that the curves for the regions between the fingers are correctly fitted: the fitted m in both cases equals the m used as input, whereas the series resistance is almost increased by a factor of 10 for the high R_{cl} case (it is slightly less than 10 because the emitter sheet resistance is kept the same for both curves). However, fitting the J - V graph for the total cell results in a large increase of m , while the series resistance almost equals the value for the low R_{cl} case. So the very non-uniform potential distribution over the cell leads to an increase of the parameters describing recombination instead of the parameter for series resistance. Note that a uniform increase of the contact resistance was correctly handled in fitting (series resistance increases, m equals m used as input), only non-uniformity leads to problems. However, the non-uniform case is found to be the most occurring one in practice.

As is clear from the example just given, it is even possible to obtain $m > 2$ by R_{cl} non-uniformity, while m should be < 2 according to the standard (1-dimensional) solar cell model. Another paper discussing the fit problems in case of large series resistance non-uniformity was published recently [12]. That paper took line interruptions or non-printed areas as possible reasons for series resistance non-uniformity, non-uniform contact resistance was not mentioned however. The reason for the fact that the normal fit model is not functioning correctly is that the potential differences over the cell are not any more small compared to the thermal voltage q/kT of 25 mV at 300 K. Therefore the correct calculation of the cell output current gets non-linear while the normal fit model that accounts for series resistance with a lumped value ρ_{series} assumes linearity.

A solution that is sometimes used to account for the fit problems just mentioned is to introduce a series resistance that is not constant, but current dependent [12]. However, it is better to avoid the use of this concept by measuring V_{oc} as a function of light intensity [2] for the quantification of series resistance influence. Using the fill factor FF_{Rs0} of the “series resistanceless” J - V curve obtained with that method, and subtracting the fill factor FF of the normal J - V curve, the influence of series resistance on the solar cell J - V curve can be easily quantified by

$$\Delta FF_{Rs} \equiv FF_{Rs0} - FF,$$

By the use of ΔFF_{Rs} , the series resistance influence is characterized by a single value which gives a direct feeling for the efficiency loss due to series resistance.

As a demonstration a normal J - V curve and the series resistanceless curve of the same cell are shown for a cell with a high contact resistance region in Fig. A.2.

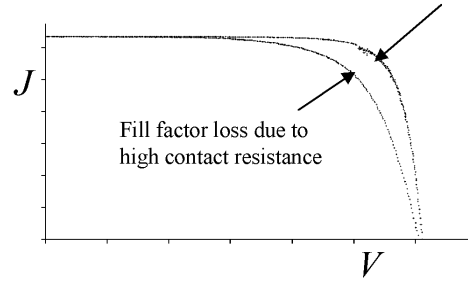


Figure A.2: Series resistanceless curve obtained from V_{oc} measurements as a function of light intensity, and the normal J - V curve. The cell is one with a high and non-uniform contact resistance, $\Delta FF_{p\sigma} = 11.3\%$.

When the FF difference between the curves is large as in the curves above, the Corescan is the appropriate method to find the locations or regions that are responsible for the fill factor loss.